Sooting Limits of Nonpremixed *n*-Heptane, *n*-Butanol, and Methyl Butanoate

Flames: Experimental Determination and Mechanistic Analysis

Sili Deng*, Jeremy A. Koch, Michael E. Mueller, Chung K. Law

Department of Mechanical and Aerospace Engineering, Princeton University, Princeton, NJ 08544, USA

Abstract

The sooting limits of nonpremixed *n*-heptane, *n*-butanol, and methyl butanoate flames were determined experimentally in a liquid pool stagnation-flow configuration. In addition, complementary simulations with detailed polycyclic aromatic hydrocarbon (PAH) chemistry and a detailed soot model, based on the Hybrid Method of Moments (HMOM), were performed and compared with the experimental critical strain rates for the sooting flames. Both experiment and simulation showed that *n*-heptane and *n*-butanol had similar sooting characteristics, while methyl butanoate had the least sooting propensity. Further sensitivity and reaction path analysis demonstrates that the three fuels share similar PAH chemical pathways, and the differences in sooting propensity lie in the fuel breakdown processes. The oxygen bounded in *n*-butanol does not reduce soot precursor concentrations but is primarily involved in intramolecular water elimination reactions. On the contrary, the fuel bound oxygen in methyl butanoate shortens the carbon chain of the

ring formation from the intermediate chain species is found to be the rate limiting step.

Keywords: Soot, Nonpremixed stagnation-flow flame, Hybrid Method of Moments, n-Butanol, Methyl butanoate

soot precursors and promotes their oxidation, which reduces the total carbon available for soot formation. C_5 and C_6

1. Introduction

The utilization of biofuels, which are potential partial replacements for liquid fuels derived from fossil fuels, is garnering wide attention not only because these fuels are renewable, locally producible, and carbon neutral [1] but also due to their potential positive impacts on particulate matter (PM) emission control. Biofuels, including bioalcohols and biodiesels, mainly consist of oxygenated hydrocarbons, such as ethers, alcohols, and esters. When used as additives in conventional diesel fuels, PM emissions have been found to decrease as oxygenated additive concentrations increase [2].

However, the role of oxygenated additives on soot emission reductions has not yet come to a scientific consensus. For example, Frijters and Baert [3] attributed the PM reduction to the fuel oxygen content, which reduced the local equivalence ratio and, by implication, the flame temperature. Westbrook *et al.* [4] performed simulations of premixed

*Corresponding Author: silideng@princeton.edu

n-heptane and oxygenates flames and found that, even with the same oxygen content, the oxygenates had distinct efficiencies in soot precursor reduction. Furthermore, Pepiot *et al.* [5] proposed a structural group contribution approach to interpret diesel engine experimental data, noting that the aromatics contained in the conventional diesel fuels have very strong sooting tendencies, which are moderated through substitution by the clear-burning oxygenated additives. Therefore, this replacement effect should be identified and quantified to reveal the role of the oxygen moieties.

Conversely, McEnally and Pfefferle [6, 7] found that butanol isomer doped methane co-flow diffusion flames produce more soot than the undoped ones and concluded that the fuel carbon number and structure were more important than the fuel bound oxygen. Similar conclusions were reached by Camacho *et al.* [8] by probing the evolution of the detailed particle size distribution function in a set of laminar premixed flames of *n*- and *i*-butane/butanol with fixed C/O ratio and maximum temperature.

Although valuable contributions have been made, well-controlled fundamental experiments and detailed chemical kinetic analyses are still needed to understand the chemical pathways for soot formation with oxygenated fuels. Moreover, since soot formation is a kinetically controlled process [9], the residence times of soot precursors are also expected to influence the sooting propensities [10], and these effects have not yet been explored in detail for oxygenated fuels. Therefore, the present experimental and computational study focuses on the sooting limits (a residence time effect) of three neat liquid diesel/biofuel components, specifically, *n*-heptane, *n*-butanol, and methyl butanoate, in a nonpremixed stagnation-flow system. A combined chemical kinetic model with detailed polycyclic aromatic hydrocarbon (PAH) chemistry is constructed to investigate the important pathways of soot formation with these three fuels. This choice of the target fuels is motivated by both practical and scientific concerns. First, butanol has more diverse non-food sources of supply than ethanol, which has been derived primarily from corn. Second, methyl butanoate is chosen not only because it is a typical biodiesel surrogate but also due to the availability of detailed chemical kinetic models. Third and most important, the boiling points of *n*-butanol and methyl butanoate are 391 K and 375 K, respectively, which are very close to that of *n*-heptane (372 K). This similarity in the vaporization characteristics enables similar fuel vapor concentrations above the stagnation liquid pool and assures similar rates of supply of the vaporized fuel to the flame region.

2. Experimental Methodology

The sooting limits of nonpremixed model diesel/biofuel components, in terms of the critical strain rate (CSR) at which soot inception starts to happen when the residence time, which is the inverse of the strain rate, is further increased, were measured at atmospheric pressure in a liquid pool stagnation-flow configuration described in detail elsewhere [11]. In the present work, an unheated oxidizer stream impinged against the liquid fuel pool, and flames were established by spark ignition. With the 20 mm pool diameter, the separation distance between the oxidizer nozzle and liquid pool was maintained at 13 mm to assure a well-characterized stagnation flow and also to enable better measurement of the velocity field by Laser Doppler Velocimetry (LDV).

Due to the oxygen content in *n*-butanol and methyl butanoate, their flame temperatures are lower than *n*-heptane. Since soot formation is highly sensitive to temperature [12], this thermal effect has to be eliminated to elucidate the chemical effects. In the present study, *n*-butanol and methyl butanoate flame temperatures were kept at the same as *n*-heptane by replacing a portion of the nitrogen in the oxidizer stream with argon, which is the same approach taken by Law and co-workers [13–15]. The amount of nitrogen replacement was calculated with CHEMKIN's equilibrium solver EQUIL [16] for stoichiometric fuel/oxidizer mixtures, and the diluent concentrations are summarized in Table. 1. Liquid *n*-heptane, *n*-butanol, and methyl butanoate were fed to the liquid pool by a syringe pump at room temperature.

Soot detection was based on luminosity observations, for Du *et al.* [13] found that such measurements agreed well with light scattering detection and were a convenient indicator of the presence of soot particles. The experimental procedure to identify the sooting limit is briefly summarized here. First, the oxidizer component flow rates were set, and a non-sooting blue flame was established. Then, the bypass valve placed upstream of the oxidizer nozzle was slowly adjusted to divert oxidizer out of the system, effectively reducing the velocity of the stream and, consequently, the strain rate. The residence time was further increased until yellow luminosity began to appear on the fuel rich side of the flame. A standard single-component LDV measurement was performed along the axial centerline under this threshold flow condition, and the local strain rate was determined as the axial velocity gradient upstream of the flame [13]. Following this procedure, the sooting limits for the three fuels with different oxygen concentrations in the oxidizer streams were identified.

3. Computational Methodology

The liquid pool stagnation-flow flames were simulated with the FlameMaster code [17], including detailed PAH chemistry and a detailed soot model. The boundary conditions on the fuel side were specified following Bui-Pham *et al.* [18]. In brief, the Antoine equation [19] was used to close the boundary value problem by relating the liquid pool surface temperature and vapor pressure, yielding a relationship for the fuel mole fraction at the surface. As in the experiment, the strain rate was determined as the gradient of the velocity profile on the oxidizer side, ahead of the flame. Furthermore, to mimic the luminosity observations, the computational CSRs were determined based on a global domain-integrated soot volume fraction (f_V). The threshold value was determined to match the experimental results of n-heptane at larger X_{O_2} cases and was kept fixed for all other cases. The qualitative trends presented in the next section were not found to be sensitive to this threshold or alternative metrics that were explored.

A detailed chemical model including PAH chemistry was combined from three well validated models corresponding to the fuels of interest. A mechanism with PAH chemistry of engine relevant fuels was developed by Blanquart, Pitsch, and co-workers [20, 21]. This mechanism has been validated extensively against experimental measurements of ignition delay times, laminar burning velocities, and species profiles in both premixed and nonpremixed flames over a large range of equivalence ratios and pressures. Of particular interests to this work, the mechanism was validated

in *n*-heptane nonpremixed flames against the measurements of Berta *et al.* [22]. In the present study, this mechanism was adopted as the base mechanism with PAH chemistry. Conversely, although efforts have been made in developing chemical kinetic models for *n*-butanol and methyl butanoate in recent years, less emphasis has been placed on their PAH pathways. Therefore, reduced oxidation/pyrolysis chemistry of *n*-butanol and methyl butanoate kinetic models was adopted from Liu *et al.* [1] and combined with the base mechanism. These models were reduced from the work of Sarathy *et al.* [23] and Gaïl *et al.* [24], respectively. The thermal and transport data of the species that appeared only in the *n*-butanol and methyl butanoate mechanism were taken from these latter works. The combined mechanism consists of 220 species and 2259 forward and backward reactions. The combined mechanism was further validated against laminar flame speed measurements [1] and compared with the predictions by the original mechanisms; results of this validation are shown in Fig. 1. The differences between the combined mechanism and the original mechanism for *n*-butanol and methyl butanoate are attributed to the differences in the base chemistry, with the combined mechanism generally giving improved agreement with the experimental measurements.

The detailed soot model is based on the Hybrid Method of Moments (HMOM) developed by Mueller *et al.* [25–27]. The detailed model describes particles with both their volume and surface area and considers particle nucleation from PAH dimers [28–30], PAH condensation, particle coagulation [26], surface growth by the HACA mechanism [31], oxidation [32, 33], and oxidation-induced fragmentation [27]. In addition, the model considers thermophoresis [34] but neglects molecular diffusion [35]. In total, four quantities are used to describe the evolution of the soot population: the total soot number density, the total soot volume, the total soot surface area, and the number density of smaller particles.

4. Results and Discussion

The critical strain rates (CSRs) corresponding to the sooting limits from the experiments and computations are shown in Fig. 2. For each set of data, the region above/left of the data corresponds to non-sooting flames, and the region below/right of the data corresponds to sooting flames. For all three fuels, the CSR increases with increasing oxygen concentration in the oxidizer stream, which has been previously characterized as a thermal effect [14]. In addition, both experiment and computation show that methyl butanoate has substantially lower CSRs compared to *n*-heptane and *n*-butanol.

It is noted that, while the global trends of the experimental and computational results agree well with their values being in the same range, minor *quantitative* differences do exist. In particular, the CSR in the model is overpredicted at low oxygen mole fractions for both *n*-heptane and *n*-butanol and underpredicted at all oxygen mole fractions for methyl butanoate. Furthermore, for all fuels, the change in CSR with oxygen mole fraction is too mild in the computations compared to the experiment. These minor *quantitative* discrepancies could be attributed to several possible causes. First, the experiment (strain rate at blue to orange luminosity) and computation (strain rate at a threshold domain-integrated volume fraction) are not comparing the same quantity, but, as note above, the observed trends

(quantitative and qualitative) did not appreciably change with the computational criterion used. Second, the experiments are subject to some degree of uncertainty, which has not been quantified in detail and could potentially make the *quantitative* agreement appear worse than reality. Finally, the fuel oxidation chemistry (see, e.g., Fig. 1) and PAH formation chemistry are still under development, and constant improvements in chemical mechanisms are always required. Nonetheless, the major *qualitative* difference is well captured by both experiment and model: methyl butanoate exhibits a substantially smaller CSR compared to *n*-heptane and *n*-butanol, which are essentially the same. The remainder of this paper explores this fundamental *qualitative* difference between the three fuels.

The lower CSRs might be due to either less soot being formed overall, since the CSR was experimentally measured and accordingly defined in computations based on the absolute value of f_V , or slower chemical pathways for soot formation that are inhibited at reduced residence times. The integrated f_V under various strain rates are shown in Fig. 3. For all three fuels, less soot is formed due to reduced residence time, and n-butanol is overall as sooty as n-heptane, while methyl butanoate is the least sooty. Therefore, the CSRs correlate with the total amount of soot formed, explaining at least in part the CSR trends. However, it remains to be seen if there are any significant differences in PAH pathways with different timescales for the three fuels that could further explain the observed trends in CSR.

To understand the distinct differences in PAH evolution between the three fuels, sensitivity and reaction path analysis was performed on a representative PAH species, naphthalene ($C_{10}H_8$). As shown in Fig. 4 and Fig. 5, naphthalene shows roughly the same sensitivities to the same reactions for each of the fuels, and the chemical pathways of naphthalene are essentially the same after the fuel cracking. Initially, fuel cracks to unsaturated C_3 to C_5 chains through H abstraction followed by β -scission reactions. These smaller molecules further decompose into allyl radicals (A- C_3H_5 , CH_2 =CH- CH_2^*) and propene (C_3H_6), which contribute to C_5 and C_6 ring formation by either combining with acetylene (C_2H_2) or forming propargyl (C_3H_3), which further combines with itself to form aromatic rings. Larger species (predominantly toluene and indene) are formed by the combination of benzene and cyclopentadiene with smaller species, such as CH_3 , C_2H_2 , and C_3H_3 . Two pathways directly contribute to naphthalene formation, namely, cyclopentadienyl (C_5H_5) radical recombination and methyl addition to indenyl (C_9H_7)

$$2C_5H_5 \Longleftrightarrow C_{10}H_8 + 2H$$

$$C_9H_7 + CH_3 \Longleftrightarrow C_{10}H_8 + 2H.$$

Although the PAH pathways for the three fuels are similar, the formation of these soot precursors from the fuel cracking processes and the relative importance of the subsequent chemical pathways of PAH growth are fuel specific. Noting the similarity in the chemical pathways beyond $A-C_3H_5$ and C_3H_6 , the fuel specific breakdown pathways that lead to the generation of these precursors are depicted in Fig. 6. For both n-heptane and n-butanol, 1-butene (P- C_4H_8) is formed from the fuel decomposition, which contributes to 25% of $A-C_3H_5$ production and strongly promotes naphthalene formation, as indicated by the sensitivity analysis in Fig. 4. Moreover, the fuel bound oxygen in n-butanol is converted into water during an intramolecular water elimination reaction and does not contribute to carbon reduction [6, 7], which explains the similar sooting behavior as n-heptane.

Conversely, C_3 species are the largest species formed from methyl butanoate cracking due to the fuel bound oxygen. As pointed out by Westbrook *et al.* [4], the double C=O bond is very difficult to break, so the carbon chain length is reduced when the C-C bond is broken due to β -scission. The oxygenated parts are then oxidized to CO and CO_2 , preventing the carbon from entering the pool for soot formation [36, 37]. As shown in Fig. 7, fewer allyl radicals are formed from methyl butanoate, such that the concentration of C_5H_5 is also reduced. Since one of the pathways for naphthalene depends quadratically on C_5H_5 , even moderate reductions in the radical concentration will significantly reduce naphthalene. As a result, in methyl butanoate flames, the C_5H_5 recombination pathway is negligible compared to the C_9H_7 pathway. This reduction in soot precursors from fuel cracking processes distinguishes methyl butanoate from *n*-heptane and *n*-butanol, in terms of the sooting propensity and CSR.

At this point, the pathways and species that are responsible for soot formation have been identified. The next question that naturally arises is how sensitive these pathways are to the increasing strain rate that leads to reduced soot formation. Although not shown here, sensitivity and reaction path analysis was conducted at critical strain rates, and no substantial differences were found compared with low strain rate cases. In addition, if the CSR is defined based on a relative metric, in other words, to be the strain rate at which the global domain-integrated f_V is 10% of the value at a fixed low strain rate (16 s⁻¹), the three fuels have essentially the same CSR, indicating the potential similarity in the rate limiting steps of soot formation. These observations indicate that it is mostly the total amount of soot formed with the three fuels that give the differences in CSR.

To elucidate the rate limiting step, profiles of soot precursors at low and critical strain rates are shown in Fig. 7. All profiles shift in the direction of the liquid pool at higher flow rates as increased strain rates push the stagnation plane towards the pool. Species with ring structures, specifically C_5H_6 and C_6H_6 have lower concentrations at CSR, responding to strain similar to f_V . However, the upstream C_3 precursors, A-C₃H₅ and C₃H₃, have higher concentrations at CSR. This indicates that these species have insufficient residence times to form rings, resulting in the observed decrease in soot. Therefore, the ring formation reactions

$$C_2H_2 + A - C_3H_5 \iff H + C_5H_6$$

 $2C_3H_3 \iff C_6H_6$

are the rate limiting steps.

5. Conclusions

In this work, *n*-heptane, *n*-butanol, and methyl butanoate were chosen as diesel, bioalcohol, and biodiesel surrogates of interest due to their similar volatilities and consequent potential applications in diesel fuel blending. Their sooting limits were measured experimentally with the stagnation-flow apparatus. Computations were conducted for the same configuration using detailed PAH chemistry and a detialed soot model based on the Hybrid Method of Moments (HMOM). Both experimental and computational results showed the critical strain rates of the three fuels, based

on the absolute soot volume fraction, increase with increasing oxygen mole fraction in the oxidizer, due to the thermal effect. Moreover, although *n*-heptane and *n*-butanol show similar sooting propensities, methyl butanoate produces significantly less soot.

Sensitivity and reaction path analysis was performed for naphthalene, the first PAH species from which soot forms. This analysis revealed that, despite different sooting tendencies, the three fuels shared similar PAH chemical pathways. C_5 , C_6 , C_7 , C_9 rings, and naphthalene are formed sequentially through the combination of C_3 and smaller chain radicals resulting from fuel cracking processes. Due to the fuel bound oxygen in methyl butanoate, less and shorter chain radicals are available for soot formation, compared with the other fuels, such that methyl butanoate forms the least soot and has the lowest critical strain rates.

The strain rate effects on soot formation were also examined. Despite different sooting propensities, for all three fuels, C_5 and C_6 ring formation reactions are the rate limiting steps. Their concentrations drop as the residence time is reduced, such that the downstream PAH chemistry is consequently inhibited, resulting in the sooting limits.

Acknowledgments

This work was supported by the Combustion Energy Frontier Research Center, an Energy Frontier Research Center funded by the US Department of Energy, Office of Basic Energy Sciences under Award Number DE-SC0001198.

References

- [1] W. Liu, A. P. Kelley, C. K. Law, Proc. Combust. Inst. 33 (2011) 995–1002.
- [2] M. S. Graboski, R. L. McCormick, Prog. Energy Combust. 24 (1998) 125–164.
- [3] P. J. M. Frijters, R. S. G. Baert, Int. J. Veh. Des. 41 (2006) 242-255.
- [4] C. K. Westbrook, W. J. Pitz, H. J. Curran, J. Phys. Chem. A 110 (2006) 6912–6922.
- [5] P. Pepiot, H. Pitsch, R. Malhotra, S. R. Kirby, A. L. Boehman, Combust. Flame 154 (2008) 191–205.
- [6] C. S. McEnally, L. D. Pfefferle, Proc. Combust. Inst. 30 (2005) 1363–1370.
- [7] C. S. McEnally, L. D. Pfefferle, Environ. Sci. Technol. 45 (2011) 2498–2503.
- [8] J. Camacho, S. Lieb, H. Wang, Proc. Combust. Inst. 34 (2013) 1853–1860.
- [9] U. Vandsburger, I. M. Kennedy, I. Glassman, Proc. Combust. Inst. 20 (1985) 1105–1112.
- [10] H. Tsuji, I. Yamaoka, Proc. Combust. Inst. 13 (1971) 723-731.
- [11] W. Liu, D. Zhu, N. Wu, C. K. Law, Combust. Flame 157 (2010) 259-266.
- [12] H. Wang, Proc. Combust. Inst. 33 (2011) 41-67.
- [13] D. X. Du, R. L. Axelbaum, C. K. Law, Proc. Combust. Inst. 22 (1989) 387-394.
- [14] D. X. Du, R. L. Axelbaum, C. K. Law, Proc. Combust. Inst. 23 (1991) 1501–1507.
- [15] R. L. Axelbaum, C. K. Law, Proc. Combust. Inst. 23 (1991) 1517–1523.
- [16] R. J. Kee, F. M. Rupley, J. A. Miller, CHEMKIN Collection, Release 3.6, Reaction Design, Inc., San Diego, CA, 2000.
- [17] H. Pitsch, FlameMaster, a C++ computer program for 0D combustion and 1D laminar flame calculations.
- [18] M. Bui-Pham, K. Seshadri, Combust. Sci. Technol. 79 (1991) 293–310.
- [19] B. E. Poling, J. M. Prausnitz, J. P. O'Connell, The Properties of Gases and Liquids, McGraw-Hill, New York, Fifth edition, 2000.
- [20] G. Blanquart, P. Pepiot, H. Pitsch, Combust. Flame 156 (2009) 588-607.

- [21] K. Narayanaswamy, G. Blanquart, H. Pitsch, Combust. Flame 157 (2010) 1879–1898.
- [22] P. Berta, S. K. Aggarwal, I. K. Puri, Combust. Flame 145 (2006) 740-764.
- [23] S. M. Sarathy, M. J. Thomson, C. Togbé, P. Dagaut, F. Halter, C. Mounaim-Rousselle, Combust. Flame 156 (2009) 852-864.
- [24] S. Gaïl, S. M. Sarathy, M. J. Thomson, P. Diévart, P. Dagaut, Combust. Flame 155 (2008) 635–650.
- [25] M. E. Mueller, G. Blanquart, H. Pitsch, Proc. Combust. Inst. 32 (2009) 785–792.
- [26] M. E. Mueller, G. Blanquart, H. Pitsch, Combust. Flame 156 (2009) 1143–1155.
- [27] M. E. Mueller, G. Blanquart, H. Pitsch, Proc. Combust. Inst. 33 (2011) 667-674.
- [28] C. A. Schuetz, M. Frenklach, Proc. Combust. Inst. 29 (2002) 2307–2314.
- [29] D. Wong, C. A. Schuetz, M. Frenklach, in: H. Bockhorn, A. D'Anna, A. Sarofim, H. Wang (Eds.), Combustion Generated fine Carbonaceous Particles, KIT Scientific Publishing, 2009, pp. 247–257.
- [30] G. Blanquart, H. Pitsch, in: H. Bockhorn, A. D'Anna, A. Sarofim, H. Wang (Eds.), Combustion Generated fine Carbonaceous Particles, KIT Scientific Publishing, 2009, pp. 439–466.
- [31] M. Frenklach, H. Wang, Proc. Combust. Inst. 23 (1991) 1559–1566.
- [32] A. Kazakov, H. Wang, M. Frenklach, Combust. Flame 100 (1995) 111–120.
- [33] K. G. Neoh, J. B. Howard, A. F. Sarofim, in: Particulate Carbon Formation during Combustion, Plenum Press, 1981, pp. 162–282.
- [34] L. Waldmann, K. H. Schmitt, in: C. N. Davies (Ed.), Aerosol Science, Academic Press, 1966.
- [35] F. Bisetti, G. Blanquart, M. E. Mueller, H. Pitsch, Combust. Flame 159 (2012) 317–335.
- [36] Q. Feng, A. Jalali, A. M. Fincham, Y. L. Wang, T. T. Tsotsis, F. N. Egolfopoulos, Combust. Flame 159 (2012) 1876–1893.
- [37] Y. L. Wang, Q. Feng, F. N. Egolfopoulos, T. T. Tsotsis, Combust. Flame 158 (2011) 1507–1519.

List of Figures

1	Mechanism validation on <i>n</i> -butanol (left) and methyl butanoate (right) laminar flame speeds, against	
	the experimental (symbols) and computational (dotted lines) results from Liu et al. [1]. $P = 1$ atm	
	and $T = 353 \text{ K.} \dots \dots$	10
2	Experimental (symbols) and computational (lines) CSRs	11
3	The responses of the integrated f_V to strain rate at $X_{O_2} = 0.2.$	12
4	Sensitivity of the maximum naphthalene mass fraction to kinetics at the strain rate of 16 s ⁻¹ and	
	$X_{O_2} = 0.2$. Left: Intermediate chain radical reactions. Right: Ring formation reactions	13
5	Chemical pathways for naphthalene formation at the strain rate of 16 s ⁻¹ and $X_{O_2} = 0.2$	14
6	Fuel specific pathways for C_3H_6 and A- C_3H_5 formation at the strain rate of 16 s ⁻¹ and $X_{O_2} = 0.2$.	
	From left to right: <i>n</i> -heptane, <i>n</i> -butanol, and methyl butanoate	
7	Key intermediate species profiles at low strain rates (16 s ⁻¹) and CSRs: $X_{O_2} = 0.2.$	16

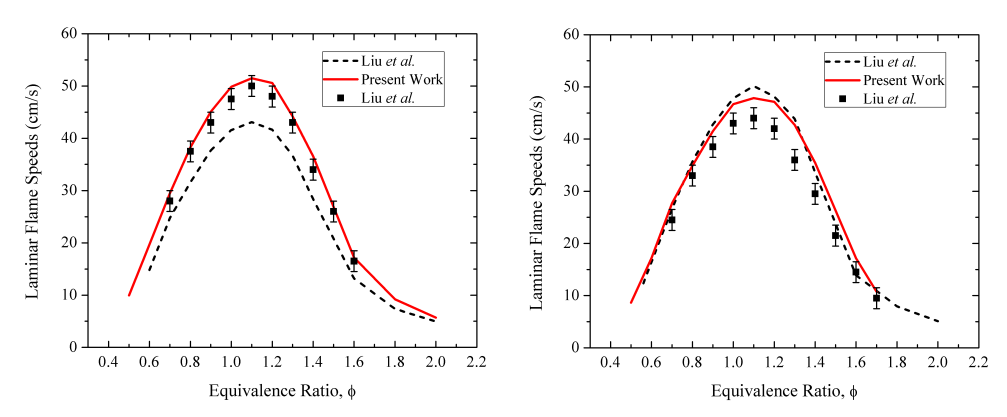
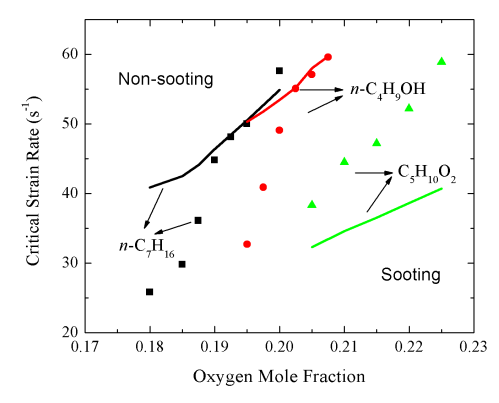


Figure 1: Mechanism validation on n-butanol (left) and methyl butanoate (right) laminar flame speeds, against the experimental (symbols) and computational (dotted lines) results from Liu $et\ al.$ [1]. P=1 atm and T=353 K.



 $Figure\ 2:\ Experimental\ (symbols)\ and\ computational\ (lines)\ CSRs.$

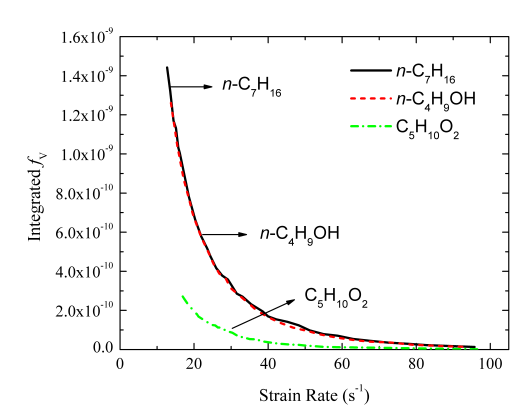


Figure 3: The responses of the integrated f_V to strain rate at $X_{{\cal O}_2}=0.2$.

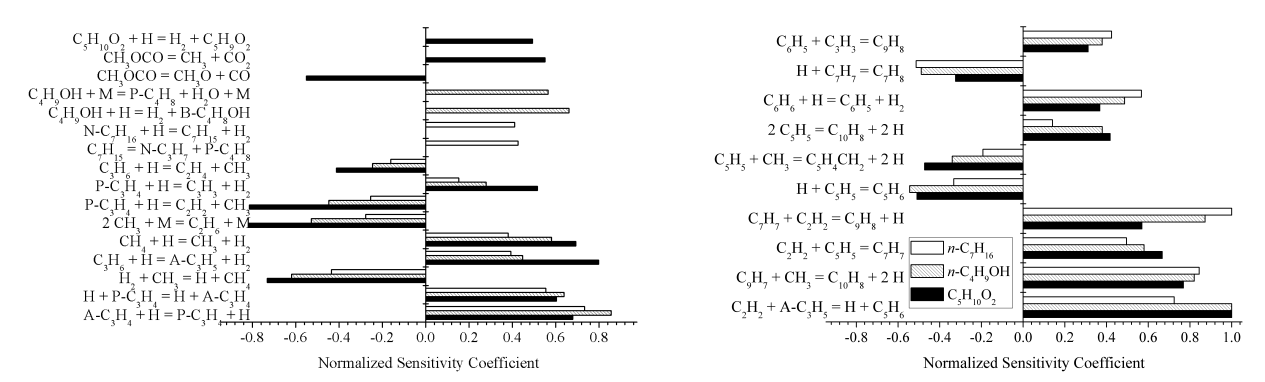


Figure 4: Sensitivity of the maximum naphthalene mass fraction to kinetics at the strain rate of 16 s⁻¹ and $X_{O_2} = 0.2$. Left: Intermediate chain radical reactions. Right: Ring formation reactions.

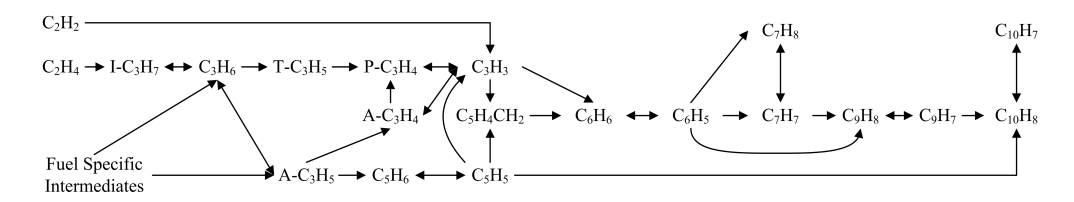


Figure 5: Chemical pathways for naphthalene formation at the strain rate of 16 s⁻¹ and $X_{O_2} = 0.2$.

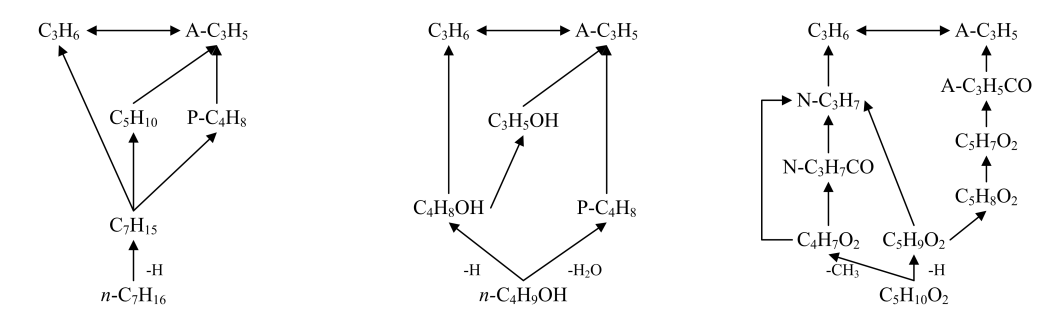


Figure 6: Fuel specific pathways for C_3H_6 and A- C_3H_5 formation at the strain rate of 16 s⁻¹ and $X_{O_2} = 0.2$. From left to right: *n*-heptane, *n*-butanol, and methyl butanoate.

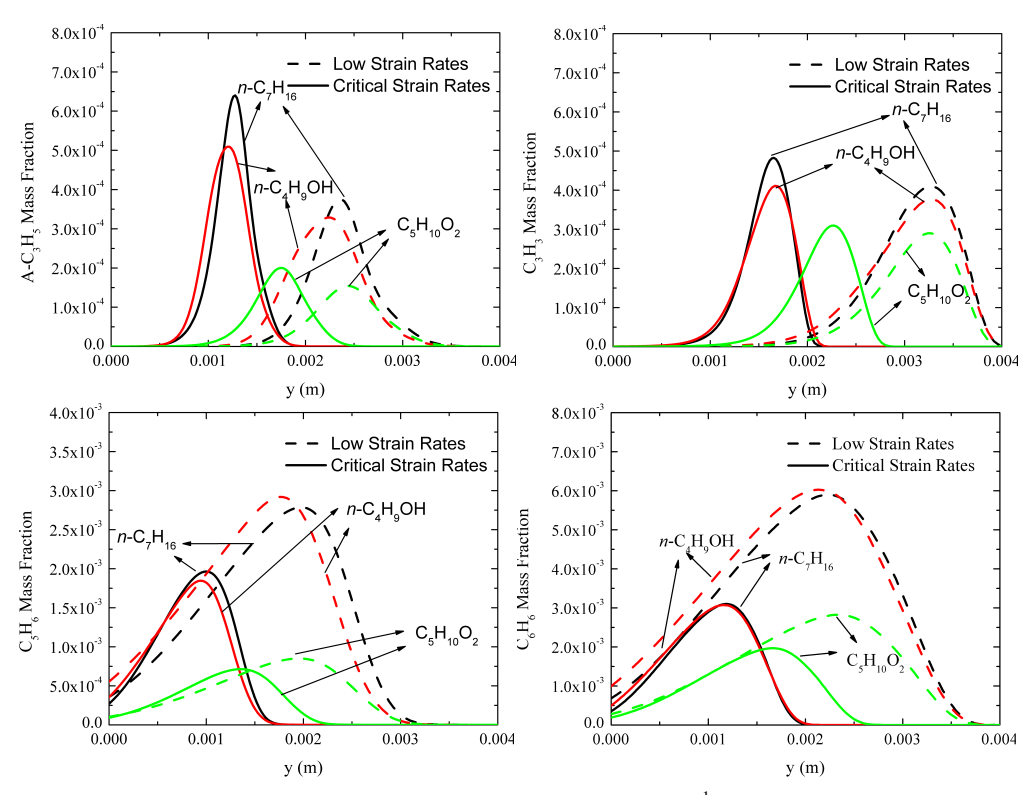


Figure 7: Key intermediate species profiles at low strain rates (16 s⁻¹) and CSRs: $X_{O_2} = 0.2$.

T	ist	Λf	To	hl	O.C.
	ASI.	an a	12	m	-

Table 1: Oxidizer stream composition in mole fractions.

	O_2										
		0.1950	0.1975	0.2000	0.2025	0.2050	0.2075	0.2100	0.2150	0.2200	0.2250
$n - C_4H_9OH$	N_2	0.7718	0.7679	0.7640	0.7600	0.7560	0.7521				
	Ar	0.0332	0.0346	0.0360	0.0375	0.0390	0.0404				
$C_5H_{10}O_2$	N_2					0.7119	0.7068	0.7017	0.6915	0.6811	0.6707
	Ar					0.0831	0.0857	0.0883	0.0935	0.0989	0.1043